Mechanics Research Communications 149 (2025) 104535

Contents lists available at ScienceDirect

Mechanics Research Communications

journal homepage: www.elsevier.com/locate/mechrescom

Adhesive contact of a viscoelastic fibrillar surface — A homogenized model ☆

I. Argatov [a,b], A. Papangelo [c,d,*]

[a] Faculty of Health and Society, Malmö University, SE-205 06, Malmö, Sweden
[b] Biofilms – Research Centre for Biointerfaces, Malmö University, SE-205 06, Malmö, Sweden
[c] TriboDynamics Lab, Department of Mechanics Mathematics and Management, Politecnico di Bari, via Orabona 4, 70126 Bari, Italy
[d] Department of Mechanical Engineering, Hamburg University of Technology, Am Schwarzenberg-Campus 1, 21073 Hamburg, Germany

ARTICLE INFO

Keywords:
Rate-independent adhesion
Schapery model
Shrimali–Lopez–Pamies (SLP) model
Fibrillar surface
Viscoelastic contact
Homogenization approach
Pull-off force
Asymptotic model

ABSTRACT

A fibrillar interface is modeled as a regular array of cylindrical micropillars bonded to a substrate, with a focus on the viscoelastic properties of the fibrils. A one-dimensional linear constitutive model describes the coupled deformation of an individual fibril and the substrate. For a compliant viscoelastic substrate, the interaction backing layer effect between fibrils through the substrate deformations is also accounted for. In the case of a viscoelastic Winkler-type foundation whose adhesive mechanism is described by the Shrimali–Lopez-Pamies criterion of maximum rate-independent elongation of the foundation elements, an exact analytical solution is derived for the displacement-controlled loading protocol. A leading-order discrete asymptotic model is developed for the Schapery-type rate-independent adhesive contact between the viscoelastic fibrillar substrate and a rigid punch. By neglecting the influence of the backing layer, a homogenized model is derived in detail. The debonding incubation time is introduced, and an analytical approximation for the pull-off force is obtained under conditions of strong adhesion and fast unloading after a long dwell time.

1. Introduction

Nature's solutions have been inspiring engineers for centuries. A striking example is the gecko lizard, renowned for its remarkable ability to run up vertical walls [1]. This phenomenon of reversible adhesion is explained by the presence of fibrillar structures covering the gecko's feet [2,3]. Gecko-inspired artificial fibrillar surfaces with enhanced adhesive properties have been developed over the past two decades [4,5] with ever-increasing research activity in recent years [6–8].

Fibrillar surfaces are typically fabricated from polymer materials [4,9], which are known not only for their adhesive surface properties but also for their bulk viscoelastic properties. A technological ability to practically realize reversible adhesion is a crucial interface functionality in various engineering fields ranging from robotics [10,11] to biomedical devices [12]. Since gecko-inspired adhesives have potential applications in soft grippers [13] and object manipulation [14], it is important to assess the viscoelastic (time-dependent) effects involved in the contact deformation of fibrillar surfaces.

Recently, the mathematical modeling of micropatterned interfaces has received increasing attention [15,16]. A progress has been also made in the understanding viscoelastic continuous [17,18] and discrete [19,20] adhesive contact, largely driven by numerical [21] and semi-analytical [22] approaches developed primarily for the three-parameter viscoelastic standard solid model. However, since the publication of a comprehensive review [23] on analytical models of bioinspired fibrillar adhesives, little advance has been achieved in the homogenization approach, as the discrete structure of these adhesives straightforwardly dictates the use of discrete spring-like modeling approaches.

In this paper, we apply a homogenization approach [24,25], developed previously for elastic contact. Since we are aiming at the development of an analytical modeling framework for experimental studies, our analysis is focused on practical details. Yet, the difficulties associated with adhesive viscoelastic contact outweigh those primarily related to the discrete nature of contact itself. That is why, in Section 2, we first briefly investigate the auxiliary problem of adhesive contact for a viscoelastic Winkler-type foundation. In Section 3, we introduce a discrete model of a viscoelastic fibrillar substrate by treating the microcontacts individually. A homogenized asymptotic model is developed in Section 4. Section 5 presents practically useful approximate analytical solutions for interpreting experimental data. Finally, in Section 6, we provide a discussion of the results and formulate our main conclusions.

☆ This article is part of a Special issue entitled: 'Discrete to Continuous Structures' published in Mechanics Research Communications.

* Corresponding author at: TriboDynamics Lab, Department of Mechanics Mathematics and Management, Politecnico di Bari, via Orabona 4, 70126 Bari, Italy.
E-mail address: antonio.papangelo@poliba.it (A. Papangelo).

https://doi.org/10.1016/j.mechrescom.2025.104535
Received 12 June 2025; Received in revised form 1 September 2025; Accepted 6 October 2025
Available online 14 October 2025

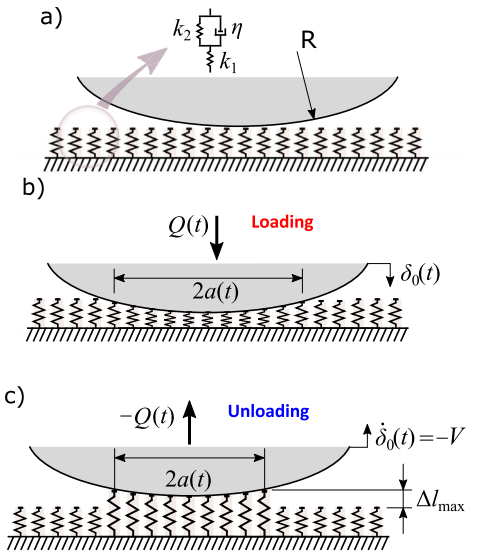

Fig. 1. Schematics of contact for a viscoelastic Winkler-type foundation: (a) Initial (unloaded) contact configuration; (b) Loaded (non-adhesive) contact; (c) Unloaded (adhesive) contact configuration.

2. Non-adhesive/adhesive contact for a viscoelastic Winkler-type foundation

We consider a foundation made of independently deforming standard-solid elements (see Fig. 1a), which is supposed to be indented with an axisymmetric rigid body (punch) of paraboloidal shape (approximating a sphere). The indentation starts at the time moment $t = 0$, and the contact zone will be characterized by a variable radius of contact, $a(t)$. Let us recall that a classical Winkler foundation (also called the Fuss–Winkler foundation [26,27]) is described by the constitutive equation $p(\mathbf{x}) = kw(\mathbf{x})$, where $p(\mathbf{x})$ is the surface pressure at the point with Cartesian coordinates $\mathbf{x} = (x_1, x_2)$, $w(\mathbf{x})$ is the local surface deflection, and k is the Winkler foundation stiffness.

For a viscoelastic Winkler-type foundation, the time-dependent constitutive equation has the form

$$p(\mathbf{x},t) = k_\infty \int_{0^-}^{t} \Psi(t-\tau)\frac{\partial w}{\partial \tau}(\mathbf{x},\tau)\,\mathrm{d}\tau, \tag{1}$$

where k_∞ is the relaxed (equilibrium) stiffness, and $\Psi(t)$ is the normalized relaxation function, such that $\Psi(t) \to 1$ as $t \to \infty$. In the case of standard-solid elements, we have $\Psi(t) = 1+\rho^{-1}(1-\rho)\exp(-t/\tau_\mathrm{R})$, where τ_R is a characteristic relaxation time, $\rho = k_\infty/k_0 < 1$, and k_0 is the instantaneous foundation stiffness (for the model configuration shown in Fig. 1a, we have $k_0 = k_1$ and $k_\infty = k_1k_2/(k_1+k_2)$).

In the special case of spherical (or, to be more precise, paraboloidal) punch of some relatively large radius, R, the kinematic contact condition can be written as

$$w(\mathbf{x},t) = \delta_0(t) - \frac{(x_1^2+x_2^2)}{2\mathrm{R}}\mathcal{H}(t), \tag{2}$$

where $\delta_0(t)$ is the punch displacement, and $\mathcal{H}(t)$ is the Heaviside function such that $\mathcal{H}(t) = 0$ for $t \le 0$ and $\mathcal{H}(t) = 1$ for $t > 0$. It is tentatively assumed that $\delta_0(t) \equiv 0$ for $t \le 0$ in accord with the initial conditions formulated above.

By integrating Eq. (1) over the circular contact zone, in view of (2), we obtain the total contact force

$$\frac{Q(t)}{\pi k_\infty} = a^2(t)\int_{0^-}^{t}\Psi(t-\tau)\dot{\delta}_0(\tau)\,\mathrm{d}\tau - \frac{a^4(t)}{4\mathrm{R}}\Psi(t). \tag{3}$$

To fix our ideas, we consider the displacement-controlled loading protocol, so that the history of the indentation is specified by the known function $\delta_0(t)$ given for $t > 0^+$ (i.e., an instantaneous jump-like indentation displacement is allowed). For instance, in the indentation relaxation experiment, we have $\delta_0(t) = \delta_{00}\mathcal{H}(t)$ for $t \in (0, t_\mathrm{m})$, where the time t_m denotes the duration of the loading phase. Then, from Eq. (3), it follows that

$$\frac{Q(t)}{\pi k_\infty} = a^2(t)\left(\delta_{00}\Psi(t) + \int_{t_\mathrm{m}}^{t}\Psi(t-\tau)\dot{\delta}_0(\tau)\,\mathrm{d}\tau\right) - \frac{a^4(t)}{4\mathrm{R}}\Psi(t), \tag{4}$$

where it is supposed that $t \ge t_\mathrm{m}$.

Further, let us consider a non-adhesive indentation loading (see Fig. 1b), when $\dot{\delta}_0(t) \ge 0$ for $t \le t_\mathrm{m}$ and $a^2(t) = 2\mathrm{R}\delta_0(t)$, and an adhesive pull-off unloading, when $\dot{\delta}_0(t) < 0$ for $t > t_\mathrm{m}$. In the latter case, we assume that the extent of the contact zone is specified by the adhesion fracture criterion of maximum rate-independent elongation of the foundation elements (see Fig. 1c) . This criterion (also called [22] the Shrimali and Lopez-Pamies (SLP) model [28]) in the context of the contact problem under consideration means that the contact radius $a(t)$ varies according to the equation

$$\delta_0(t) - \frac{a^2(t)}{2\mathrm{R}} = -\Delta l_{\max}, \tag{5}$$

where $\Delta l_{\max}$ is a constant having the dimension of length.

It should be noted here that a rate-dependent increase in both fracture toughness and adhesion energy is observed in many fibrillar soft rubberlike or biological materials [29–31]. The SPG model [28] can be regarded as one of the simplest models for a fibrillar adhesive [22], and, in particular, it can predict the dependence of pull-off force on compressive preload [20].

We would like to emphasize that Eq. (5) is applied for any critical state. For instance, if the unloading phase starts from the time moment t_m when the contact radius equals $a_\mathrm{m} = \sqrt{2\mathrm{R}\delta_{00}}$ with $\delta_{00} = \delta_0(t_\mathrm{m})$ being the maximum indentation depth, then we have $\delta_0(t_\mathrm{m}) - a^2(t_\mathrm{m})/(2\mathrm{R}) = -\Delta l_{\max}$ and $a(t) \equiv a_\mathrm{m}$ for $t \in (t_\mathrm{m}, t_\mathrm{inc})$ with t_inc denoting the time moment when Eq. (5) is fulfilled for the first time, i.e., $\delta_0(t_\mathrm{inc}) - a_\mathrm{m}^2/(2\mathrm{R}) = -\Delta l_{\max}$.

In the practically interesting case of constant-rate unloading, when $\dot{\delta}_0(t) = -V$ and $\delta_0(t) = \delta_{00} - V(t-t_\mathrm{m})$ for $t > t_\mathrm{m}$, we readily find that

$$a(t) = a_\mathrm{m}\sqrt{1 - \frac{V}{\delta_{00}}(t-t_\mathrm{inc})}, \quad t > t_\mathrm{inc}. \tag{6}$$

In other words, the time evolution of the contact radius in the case of displacement-controlled adhesive unloading that follows the SLP model is completely independent of the viscoelastic properties of the deformable foundation. It should be stressed that this phenomenon is a direct consequence of the adopted adhesive fracture criterion (5). It is clear that the result would be different if the initiation of adhesive debonding is formulated, for example, in terms of the admissible maximum absolute value of the tensile contact pressure.

Let us introduce the dimensionless variables

$$\tilde{\delta}_0(\tilde{t}) = \frac{\delta_0(t)}{\delta_{00}}, \quad \tilde{a}(\tilde{t}) = \frac{a(t)}{\sqrt{2\mathrm{R}\delta_{00}}}, \quad \tilde{Q}(\tilde{t}) = \frac{Q(t)}{2\pi\mathrm{R}\delta_{00}^2 k_\infty}, \quad \tilde{t} = \frac{t}{\tau_\mathrm{R}}, \tag{7}$$

where τ_R is the characteristic relaxation time.

Then, Eqs. (4)–(6) can be represented as

$$\tilde{Q}(\tilde{t}) = \tilde{a}^2(\tilde{t})\left(\Psi(\tilde{t}) - \frac{1}{\epsilon_1}\int_{\tilde{t}_\mathrm{m}}^{\tilde{t}}\Psi(\tilde{t}-\tilde{\tau})\,\mathrm{d}\tilde{\tau}\right) - \frac{\tilde{a}^4(\tilde{\tau})}{2}\Psi(\tilde{t}), \tag{8}$$

where $\tilde{t} > \tilde{t}_\mathrm{m}$,

$$\tilde{\delta}_0(\tilde{t}) - \tilde{a}^2(\tilde{t}) = -\frac{1}{\epsilon_0}, \quad \tilde{a}(\tilde{t}) = \sqrt{1 - \frac{1}{\epsilon_1}(\tilde{t}-\tilde{t}_\mathrm{inc})}, \tag{9}$$

where $\tilde{t} > \tilde{t}_\mathrm{inc}$, and we have introduced the notation

$$\epsilon_0 = \frac{\delta_{00}}{\Delta l_{\max}}, \quad \epsilon_1 = \frac{\delta_{00}}{V\tau_\mathrm{R}}. \tag{10}$$

Thus, the evolution of the dimensionless total contact force during the debonding process, $\tilde{t} \in (\tilde{t}_\mathrm{inc}, \tilde{t}_\mathrm{end})$ where $\tilde{t}_\mathrm{end} = t_\mathrm{end}/\tau_\mathrm{R}$ and $t_\mathrm{end} =$

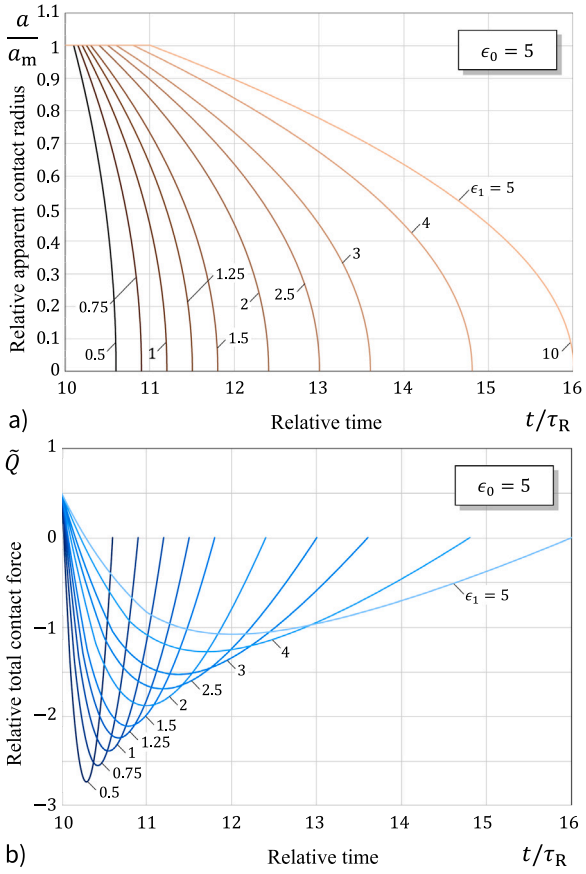

Fig. 2. Effect of the unloading rate after a long dwelling time ($t_m = 10\tau_R$): (a) Variation of the apparent contact radius; (b) Variation of the contact force.

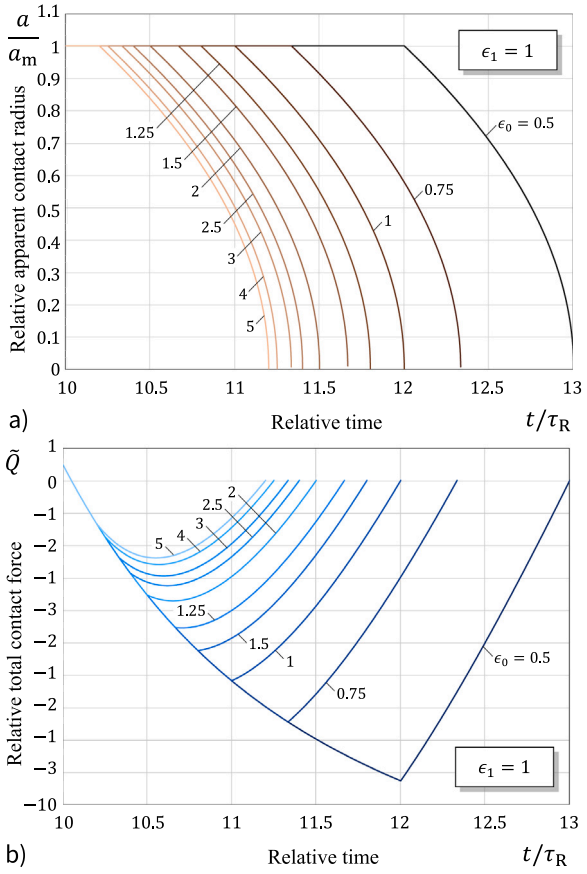

Fig. 3. Effect of the adhesion strength: (a) Variation of the apparent contact radius; (b) Variation of the contact force.

$t_{inc} + \delta_{00}/V$, is governed by the two dimensionless parameters (10). Namely, ϵ_0 is responsible for the effect of preload, and ϵ_1 characterizes the effect of unloading rate.

Figs. 2 and 3 illustrate the behavior of the spherical adhesive contact for a viscoelastic Winkler-type foundation in the unloading stage after a long dwelling time. In the numerical calculations, we simply put $t_m = 10\tau_R$ for the ease of the time scaling. The relaxation/instantaneous moduli ratio is fixed, $\rho = 0.1$.

As it is seen from Fig. 3b, the effect of unloading rate manifests itself in changing the time position of the pull-off moment from some point inside the interval (t_{inc}, t_{end}) for slow unloading regimes to the moment t_{inc}, for fast unloading regimes.

Fig. 4 shows typical force–displacement cures (force versus displacement) in the unloading stage. During the punch retrieval with an unloading velocity $\dot{\delta}_0(t) \equiv -V$, the punch displacement $\delta_0(t)$ changes from the maximum indentation depth δ_{00} to some final value $\delta_0(t_{end})$, which is negative. From Eqs. (5) and (6), it immediately follows that $t_{end} = t_m + (\Delta l_{max} + \delta_{00})/V$ and $\delta_0(t_{end}) = -\Delta l_{max}$. For slow unloading regimes, the pull-off force, Q_{off}, is determined by the local minimum of the smooth force–displacement curve, whereas for fast unloading regimes we have $Q_{off} = Q_{inc}$, where $Q_{inc} = Q(t_{inc})$. In other words, we recall that the pull-off force Q_{off} is defined as a global minimum (global maximum of the absolute value) of $Q(t)$, and therefore, the occurrence of the pull-off event can be manifested as a local minimum of a smooth or non-smooth part force–displacement curve, depending on the punch retrieval speed. The non-smoothness of the force–displacement curve is caused by the indentation mode switching.

3. Discrete viscoelastic model for a fibrillar surface

We consider a viscoelastic layer (henceforth, called the backing layer or, simply, the substrate) of finite thickness, H, bonded to a rigid base (see Fig. 5a). The substrate surface is assumed to be covered with a fine regular structure of cylindrical micropillars (sometimes, also called fibrils). For the sake of simplicity, we assume that the micropillars are made of the same material as the substrate. In a general case of dissimilar materials, an additional assumption regarding the condition of bonding at the pillar/substrate interface should be formulated.

Moreover, to simplify the consideration, we restrict our attention to the case of isotropic viscoelastic materials with a constant Poisson's ratio, ν. Then, the time-dependent stiffness properties of the substrate and micropillars will be additionally characterized by the reduced relaxed modulus, E^*_∞, and the normalized creep function, $\Phi(t)$.

The time-dependent deformation of the jth individual fibril will be described by the one-dimensional model. Let $P_j(t)$ and $\delta^j_f(t)$ denote the axial load transferred by the jth fibril and the compressive displacement, respectively, (see Fig. 6a). Then the linear theory of viscoelasticity implies the force–displacement relation

$$\delta^j_f(t) = \frac{1}{\lambda_f E^*_\infty} \int_{0-}^{t} \Phi(t-\tau) \frac{dP_j}{d\tau}(\tau)\, d\tau, \tag{11}$$

where λ_f is a stiffness coefficient having the dimension of length, and 0^- denotes the time moment preceding the onset of contact. In the particular case of relatively long cylindrical micropillars (of radius b and height l), we approximately have $\lambda_f = \pi b^2(1-\nu^2)/l$ (see Fig. 6b).

Strictly speaking, the constitutive equation (11) of the one-dimensional model for the fibril deformation characterizes the longitudinal

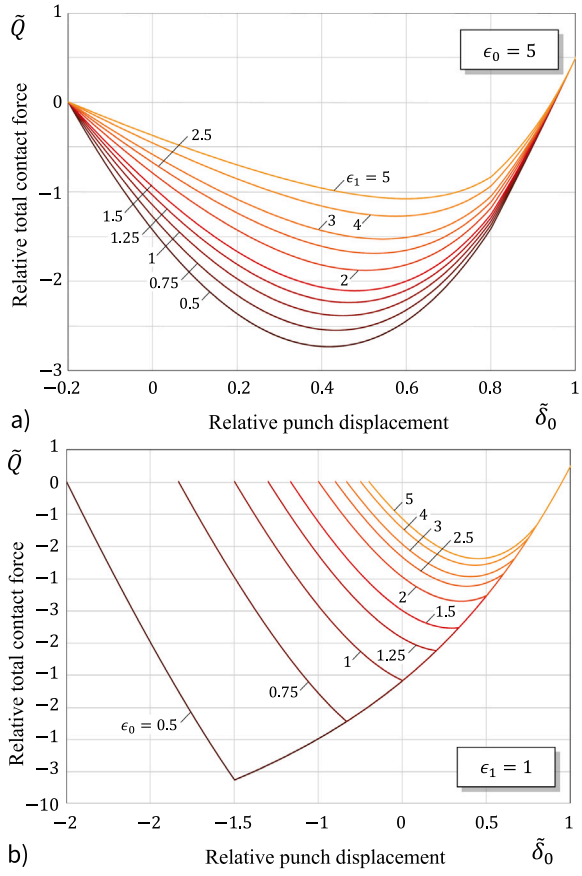

Fig. 4. Force–displacement relation upon unloading after a long dwelling time ($t_m = 10\tau_R$): (a) Effect of the unloading rate; (b) Effect of the adhesion strength.

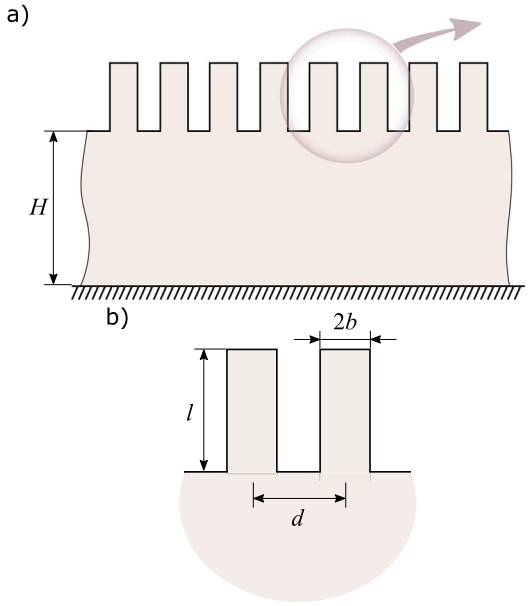

Fig. 5. (a) Geometry schematics of a fibrillar surface on a viscoelastic substrate. (b) Geometry of neighboring individual cylindrical micropillars.

deformation of an individual (separated from the substrate) micropillar compressed between two rigid plates (see Fig. 6a), when the boundary layer effects are neglected according to Saint Venant's principle. When

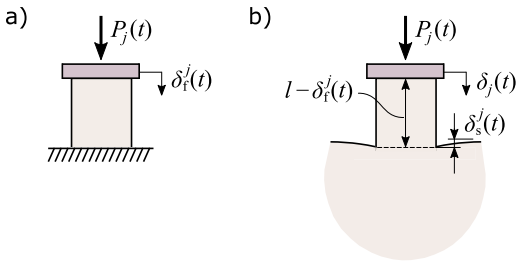

Fig. 6. Schematics of the individual fibril's loading: (a) One-dimensional model of fibrillar's deformation; (b) Deformed (loaded) configuration.

the top of the same micropillar is loaded via a rigid plate, while the micropillar being attached to the visacoelastic substrate, the substrate's deformation should be accounted as well (see Fig. 6b) by means of the vertical displacement, $\delta_s^j(t)$, of the micropillar's bottom. Based on the analysis of the corresponding elastic problem [32,33], we can write

$$\delta_s^j(t) = \frac{1}{\lambda_s E_\infty^*} \int_{0^-}^{t} \Phi(t-\tau) \frac{\mathrm{d}P_j}{\mathrm{d}\tau}(\tau)\,\mathrm{d}\tau, \tag{12}$$

where λ_s is a substrate stiffness coefficient, which is proportional to the micropillar's radius b and depends on the substrate Poisson's ratio ν.

Finally, the contact interaction effect between the micropillars (when loaded collectively by means of a large rigid punch) can be introduced via the non-diagonal terms of the substrate compliance matrix [15] as

$$\delta_{\mathrm{int}}^j(t) = \sum_{k\neq j} \frac{c_{jk}}{E_\infty^*} \int_{0^-}^{t} \Phi(t-\tau) \frac{\mathrm{d}P_k}{\mathrm{d}\tau}(\tau)\,\mathrm{d}\tau, \tag{13}$$

where c_{jk} are the compliance coefficients that are inversely proportional to the micropillar characteristic size b and depend on the distance, d_{jk}, between the centers of the jth and kth micropillars in a nonlinear way.

We observe that the constant coefficients λ_f, λ_s, and c_{jk} are supposed to be recovered from the solutions of the appropriate elastic problems, and a number of approximations are available in the literature [33–35], depending on the simplifying assumptions about the system (fibrillar surface/substrate).

Thus, if all fibrils ($j = 1, 2, \ldots, N$, where N is the number of fibrils/micropillars) are individually loaded by a system of time-dependent forces $P_1(t), P_2(t), \ldots, P_N(t)$, applied to the top surfaces of the micropillars by means of disconnected flat punches, then, according to Eqs. (11)–(13), the micropillar tops will receive the total vertical displacements

$$\delta_j(t) = \delta_f^j(t) + \delta_s^j(t) + \delta_{\mathrm{int}}^j(t), \tag{14}$$

where the terms on the right-hand side are responsible for the individual micropillar deformation, the local substrate deformation, and the substrate contact interaction, respectively.

The sum of all the time-dependent microcontact forces,

$$Q(t) = P_1(t) + P_2(t) + \cdots + P_N(t), \tag{15}$$

represents the total contact force.

3.1. Non-adhesive discrete viscoelastic contact

We consider the frictionless and non-adhesive contact of a rigid body (indenter/punch), whose surface in the initial (unloaded) state is described by the equation $z = -f(x_1, x_2)$ in terms of the shape function, $f(\mathbf{x})$ in the Cartesian coordinates $\mathbf{x} = (x_1, x_2)$ and z (see Fig. 7a, where the initial contact configuration for a convex punch is shown). The shape function of the punch may be assumed to be convex, so that the contact spots will be grouped into one cluster. We put $f(\mathbf{0}) = 0$ and $f(\mathbf{x}) \geq 0$.

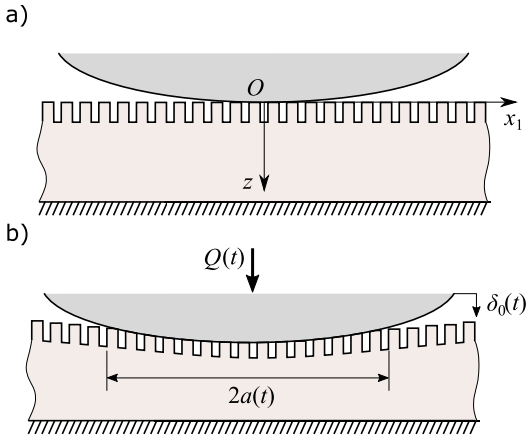

Fig. 7. Schematics of discrete contact: (a) Initial (unloaded) contact configuration; (b) Loaded (current) contact configuration.

In what follows, we consider the displacement-controlled loading protocol, assuming that the indenter displacement, $\delta_0(t)$, is a given function of time t. Since the indenter is supposed to move vertically, the equation $z = \delta_0(t) - \mathcal{H}(t)f(\mathbf{x})$ will describe the indenter surface in the current contact configuration for $t > 0$ (see Fig. 7b). Also, the zero initial conditions, including the equation $\delta_0(t) = 0$ for $t \le 0$, are tentatively assumed.

Since the contact of the indenter with the fibrillar surface is discrete and assumed to be unilateral, we write out the Signorini conditions in the form

$$P_j(t) \ge 0, \quad j = 1, 2, \dots, N, \tag{16}$$

$$P_j(t) = 0 \quad \Longrightarrow \quad \delta_0(t) - \mathcal{H}(t)f(\mathbf{x}^j) \le \delta_j(t), \tag{17}$$

$$P_j(t) > 0 \quad \Longrightarrow \quad \delta_0(t) - \mathcal{H}(t)f(\mathbf{x}^j) = \delta_j(t). \tag{18}$$

Here, $P_j(t)$ is the microcontact force that acts on the jth micropillar, and $\delta_j(t)$ is the micropillar top's displacement as modeled by Eqs. (11)–(14), and $\mathbf{x}^j = (x_1^j, x_2^j)$ is the center of location of the jth micropillar.

The inequalities (16) guarantee that the contact between the indenter and the fibrillar surface is non-adhesive (as the negatives values of the microcontact forces are not allowed). At the same time, Eq. (18) states that the displacement $\delta_j(t)$ of the top surface of the jth micropillar with the in-plane Cartesian coordinates x_1^j and x_2^j is determined by the indenter's displacement $\delta_0(t) - f(\mathbf{x}^j)$ at the point (x_1^j, x_2^j).

Finally, according to Eqs. (11)–(14), we have

$$\delta_j(t) = \frac{c_0}{E_\infty^*}\int_{0^-}^{t} \Phi(t-\tau)\frac{\mathrm{d}P_j}{\mathrm{d}\tau}(\tau)\,\mathrm{d}\tau + \sum_{k\ne j}\frac{c_{jk}}{E_\infty^*}\int_{0^-}^{t}\Phi(t-\tau)\frac{\mathrm{d}P_k}{\mathrm{d}\tau}(\tau)\,\mathrm{d}\tau, \tag{19}$$

where $j = 1, 2, \dots, N$, and we have introduced the notation $c_0 = 1/\lambda_\mathrm{f} + 1/\lambda_\mathrm{s}$ for the fibril/substrate compliance coefficient.

4. Homogenized asymptotic model

In this section, we neglect the effect of the backing layer interaction, so that Eq. (19) simplifies as

$$\delta_j(t) = \frac{c_0}{E_\infty^*}\int_{0^-}^{t}\Phi(t-\tau)\frac{\mathrm{d}P_j}{\mathrm{d}\tau}(\tau)\,\mathrm{d}\tau. \tag{20}$$

Let A_e denote the so-called elementary area (that is, the area of the periodic cell occupied by individual micropillar). So far, the periodic structure of the fibrillar interface was not exploited in the analysis. Now, we emphasize that the micropillars are deposited onto a rigid base (see Fig. 8), forming a certain simple lattice structure (e.g., square of hexagonal).

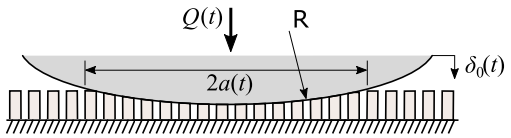

Fig. 8. Schematics of the loaded contact configuration for a fibrillar surface on a rigid base.

Following [33], we homogenize the discrete model and introduce the average contact pressure, $p(\mathbf{x}, t)$, as

$$p(\mathbf{x}^j, t) \simeq \frac{P_j(t)}{A_\mathrm{e}}, \tag{21}$$

so that, according to Eq. (15), the total contact force will be

$$Q(t) = \sum_{j=1}^{N} P_j(t) \simeq \iint_{\omega(t)} p(\mathbf{x}, t)\,\mathrm{d}\mathbf{x}, \tag{22}$$

where $\omega(t)$ is the current apparent contact area.

In view of (20) and (21), the contact condition (18) now takes the integral (averaged) form

$$\frac{\bar{c}_0}{E_\infty^*}\int_{0^-}^{t}\Phi(t-\tau)\frac{\partial p}{\partial \tau}(\mathbf{x}, \tau)\,\mathrm{d}\tau = \delta_0(t) - \mathcal{H}(t)f(\mathbf{x}), \tag{23}$$

where $\mathbf{x} \in \omega(t)$, and $\bar{c}_0 = c_0 A_\mathrm{e}$ is a compliance constant having the physical dimension of length.

To further simplify the consideration, we restrict our analysis to the special but very practical case of a spherical indenter, adopting the paraboloidal shape function

$$f(\mathbf{x}) = \frac{1}{2\mathsf{R}}(x_1^2 + x_2^2), \tag{24}$$

where R is the indenter radius.

Under the assumption that the right-hand side of Eq. (23) depends solely on the polar radius $r = \sqrt{x_1^2 + x_2}$, the apparent contact area $\omega(t)$ will be circular, i.e., $r \le a(t)$, and its evolution will be described by the variation of the contact radius $a(t)$. In such a case, the contact pressure will be axisymmetric, $p(r, t)$, so that the equilibrium equation (22) takes the form

$$Q(t) = 2\pi\int_0^{a(t)} p(\rho, t)\rho\,\mathrm{d}\rho. \tag{25}$$

Still, the contact problem formulation requires to specify the type of contact (non-adhesive or adhesive). The experimental evidence (see, e.g., [36]) shows that the loading stage, when the contact zone monotonically increases, can be regarded as a manifestation of non-adhesive contact, when the contact pressure is supposed to vanish at the contact contour, that is

$$p(a(t), t) = 0. \tag{26}$$

The contact between the indenter and the adhesive fibrillar surface in the unloading stage according to several recent studies should be treated as adhesive rate-dependent.

4.1. Non-adhesive loading

The axisymmetric problem of unilateral, non-adhesive, monotonically increasing contact for a viscoelastic Winkler-type foundation, which is mathematically equivalent to Eqs. (23)–(26), was considered previously in the literature. Here we make use of the results obtained in [37], where additional references are given. It should be noted that, though the simple case under consideration is similar to the unilateral

viscoelastic contact problems [38–40], the solution for a viscoelastic Winkler-type foundation does not follow from those for a viscoelastic half-space.

The contact force–displacement relation is given by

$$Q(t) = \frac{\pi \mathrm{R} E^*_\infty}{\bar{c}_0} \int_{0-}^{t} \Psi(t-\tau) \frac{\mathrm{d}}{\mathrm{d}\tau} [\delta_0(\tau)]^2 \mathrm{d}\tau, \tag{27}$$

where $\Psi(t)$ is the normalized relaxation function.

The inverse relation follows from Eqs. (27) in the form

$$\delta_0(t) = \left(\frac{\bar{c}_0}{\pi \mathrm{R} E^*_\infty} \int_{0-}^{t} \Phi(t-\tau) \dot{Q}(\tau)\, \mathrm{d}\tau \right)^{1/2}, \tag{28}$$

where $\dot{Q}(t)$ is the time derivative of the contact force $Q(t)$, i.e., $\dot{Q} = \mathrm{d}Q(t)/\mathrm{d}t$.

At the same time, the contact radius is given by

$$a(t) = \sqrt{2\mathrm{R}\delta_0(t)}. \tag{29}$$

In the case of force-controlled loading, when the total contact force $Q(t)$ is known, the relation between the *a priori* contact radius and the contact force $Q(t)$ is simply derived by the substitution of (28) into Eq. (29).

Finally, the contact pressure varies according to the following formula [37]:

$$\frac{\bar{c}_0}{E^*_\infty} p(r,t) = \left(\delta_0(0^+) - \frac{r^2}{2\mathrm{R}} \right) \Psi(t) \mathcal{H}\big(a(0^+) - r\big) + \int_{t_*(r)}^{t} \Psi(t-\tau) \dot{\delta}(\tau)\, \mathrm{d}\tau. \tag{30}$$

Here, $t_*(r)$ is the time when the contact contour first reaches the points with the polar radius r measured from the center of the contact area, i.e., $t_*(r) = 0$ for $0 \le r \le a(0^+)$ and $\delta(t_*) = r^2/(2\mathrm{R})$ otherwise.

4.1.1. Stepwise force-controlled loading

We assume that

$$Q(t) = Q_0 \mathcal{H}(t). \tag{31}$$

Then, the substitution of (31) into Eq. (28) yields

$$\delta_0(t) = \left(\frac{\bar{c}_0 Q_0}{\pi \mathrm{R} E^*_\infty} \Phi(t) \right)^{1/2} \mathcal{H}(t), \tag{32}$$

so that, in view of (29), we readily get

$$a(t) = \left(\frac{4\mathrm{R}\bar{c}_0 Q_0}{\pi E^*_\infty} \Phi(t) \right)^{1/4} \mathcal{H}(t). \tag{33}$$

According to Eq. (33), we have $a(0^+) > 0$ and $a(t)$ monotonically increases to the limiting value $a(\infty) = (4\mathrm{R}Q_0\bar{c}_0/\pi E^*_\infty)^{1/4}$.

4.1.2. Stepwise displacement-controlled loading

Now, we put

$$\delta_0(t) = \delta_{00} \mathcal{H}(t), \tag{34}$$

and the substitution of (34) into Eq. (27) gives

$$Q(t) = \frac{\pi \mathrm{R} E^*_\infty}{\bar{c}_0} \delta_{00}^2 \Psi(t) \mathcal{H}(t). \tag{35}$$

At the same time, Eq. (29) implies that

$$a(t) = \sqrt{2\mathrm{R}\delta_{00}} \mathcal{H}(t), \tag{36}$$

or in other words, the contact radius keeps the instantaneously obtained value $\sqrt{2\mathrm{R}\delta_{00}} = a(0^+)$.

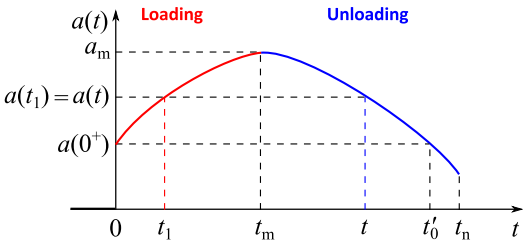

Fig. 9. A stepwise non-monotonic variation of the contact radius with a single maximum.

4.2. Non-adhesive unloading

As it was shown in the previous two subsections, a stepwise loading causes a jump-like variation of the contact radius (see Fig. 9). We note that in the case of displacement-controlled loading, we have $a(t) \equiv a(0^+) = a_\mathrm{m}$, where $a_\mathrm{m} = \max a(t)$.

Let us introduce the notation

$$w_0(r,t) = \delta_0(t) - \mathcal{H}(t) \frac{r^2}{2\mathrm{R}}. \tag{37}$$

Then, in view of (37), Eq. (23) can be rewritten in the form

$$\frac{\bar{c}_0}{E^*_\infty} \int_{0-}^{t} \Phi(t-\tau) \frac{\partial p}{\partial \tau}(r,\tau)\, \mathrm{d}\tau = w_0(r,t), \quad r \le a(t). \tag{38}$$

The unloading stage starts from the time moment $t = t_\mathrm{m}$, and we may assume that the contact pressure $p(r,t)$ is known in the loading stage $t \in (0, t_\mathrm{m})$. This prompts us to rewrite Eq. (38) as follows [37]:

$$\frac{\bar{c}_0}{E^*_\infty} p(r,t) = \int_{0-}^{t_\mathrm{m}} \Psi(t-\tau) \frac{\partial w_0}{\partial \tau}(r,\tau)\, \mathrm{d}\tau + \int_{t_\mathrm{m}}^{t} \Psi(t-\tau) \frac{\partial w_0}{\partial \tau}(r,\tau)\, \mathrm{d}\tau. \tag{39}$$

As it was shown previously [37], in view of (37), Eq. (39) can be represented in the form

$$\frac{\bar{c}_0}{E^*_\infty} p(r,t) = \int_{0-}^{t_\mathrm{m}} \Psi(t-\tau) \frac{\partial}{\partial \tau} \left(\delta_0(\tau) - \mathcal{H}(\tau) \frac{r^2}{2\mathrm{R}} \right)_+ \mathrm{d}\tau + \int_{t_\mathrm{m}}^{t} \Psi(t-\tau) \dot{\delta}_0(\tau)\, \mathrm{d}\tau, \quad r < a(t), \tag{40}$$

where $(x)_+ = (x + |x|)/2$ is the positive part function, and the first term on the right-hand side of Eq. (40) is already known.

The integration of Eq. (40) over the contact area, with Eq. (25) being taken into account, yields

$$\frac{\bar{c}_0}{\pi E^*_\infty} Q(t) = a^2(t) \int_{0-}^{t} \Psi(t-\tau) \dot{\delta}_0(\tau)\, \mathrm{d}\tau - \frac{a^4(t)}{4\mathrm{R}} \Psi(t), \tag{41}$$

where we put $a^n(t) = [a(t)]^n$.

The above equation relates the three variables $Q(t)$, $\delta_0(t)$, and $a(t)$. Yet another equation can be derived by imposing the restriction that the right-hand side of Eq. (40) is positive inside the contact area and vanishes at $r = a(t)$.

In this section, we have derived a general solution for non-adhesive unloading allowing for a jump-like variation of the contact radius as well as a dwelling time (by the corresponding specifying the indentation function $\delta_0(t)$). Next, we consider a couple of specific examples for stepwise loading to illustrate the constructed general solution.

4.2.1. Non-adhesive unloading after a stepwise displacement-controlled loading

In light of (34), Eq. (40) can be simplified as

$$\frac{\bar{c}_0}{E^*_\infty}p(r,t) = \Psi(t)\Big(\delta_{00} - \frac{r^2}{2\mathrm{R}}\Big)_+ + \int_{t_\mathrm{m}}^{t} \Psi(t-\tau)\dot{\delta}_0(\tau)\,\mathrm{d}\tau, \quad r \le a(t). \tag{42}$$

In the case under consideration, the contact area in the loading stage remains constant (see Eq. (36)), and therefore, $a(t) < a_\mathrm{m}$ for $t > t_\mathrm{m}$, when $a_\mathrm{m} = \sqrt{2\mathrm{R}\delta_{00}}$.

Hence, the boundary condition $p(r,t) = 0$ for $r = a(t)$ can be written in the form

$$\Psi(t)\Big(\delta_{00} - \frac{[a(t)]^2}{2\mathrm{R}}\Big) + \int_{t_\mathrm{m}}^{t} \Psi(t-\tau)\dot{\delta}_0(\tau)\,\mathrm{d}\tau = 0, \tag{43}$$

from where it follows that

$$a(t) = \sqrt{2\mathrm{R}}\left(\delta_{00} + \frac{1}{\Psi(t)}\int_{t_\mathrm{m}}^{t} \Psi(t-\tau)\dot{\delta}_0(\tau)\,\mathrm{d}\tau\right)^{1/2}. \tag{44}$$

We note that since $\Psi(t)$ is a positive function, the right-hand side of Eq. (44)) monotonically decreases during the unloading stage where $\dot{\delta}_0(t) < 0$.

4.2.2. Non-adhesive unloading after a stepwise force-controlled loading

In view of Eq. (29) (see also Eqs. (32) and (33)), we can transform Eq. (40) as

$$\frac{\bar{c}_0}{E^*_\infty}p(r,t) = \frac{1}{2\mathrm{R}}\int_{0^-}^{t_\mathrm{m}} \Psi(t-\tau)\frac{\partial}{\partial\tau}\Big([a(\tau)]^2 - r^2\mathcal{H}(\tau)\Big)_+\mathrm{d}\tau + \int_{t_\mathrm{m}}^{t} \Psi(t-\tau)\dot{\delta}_0(\tau)\,\mathrm{d}\tau, \quad r < a(t). \tag{45}$$

Let $t_1(t)$ be the time moment (in the loading stage) such that the current contact radius $a(t)$ (monitored in the unloading stage) is equal top the prior contact radius $a(t_1)$ (looked for in the loading stage) as shown in Fig. 9. Then, for $t \in (t_\mathrm{m}, t'_0)$, the contact pressure positivity condition follows from Eq. (45) in the form

$$0 = \frac{1}{2\mathrm{R}}\int_{t_1(t)}^{t_\mathrm{m}} \Psi(t-\tau)\frac{\partial}{\partial\tau}\Big([a(\tau)]^2 - [a(t)]^2\Big)\,\mathrm{d}\tau + \int_{t_\mathrm{m}}^{t} \Psi(t-\tau)\dot{\delta}_0(\tau)\,\mathrm{d}\tau. \tag{46}$$

In the time interval $t \in (t'_0, t_\mathrm{n})$ (see Fig. 9), the decreasing contact area enters the instantaneous contact zone $r < a(0^+)$ and, as it was shown in [37], the contact radius is determined by the equation

$$a(t) = \sqrt{2\mathrm{R}}\left(\delta_0(0^+) + \frac{1}{\Psi(t)}\int_{0^-}^{t} \Psi(t-\tau)\dot{\delta}_0(\tau)\,\mathrm{d}\tau\right)^{1/2}, \tag{47}$$

where, in view of (32), we have $\delta_0(0^+) = \big(\bar{c}_0 Q_0 \Phi(0)/E^*_\infty \pi\mathrm{R}\big)^{1/2}$.

5. Adhesive unloading

It is reasonable to assume (see, e.g., [41]) that the variation of the main contact variables during the loading stage of a punch in contact with an adhesive fibrillar surface is practically the same as that in the non-adhesive case. Namely, the jump-like phenomenon in establishing a first contact, which can be usually observed as a manifestation of Wan der Vaals forces, can be ignored in estimating the effect of preload. Hence, we may introduce the adhesion effect into our modeling framework from the unloading stage.

5.1. Schapery's model for detachment of individual fibrils

It is well known that a point of view on the fracture process as an appearance of new surfaces accompanied by an elastic energy release dates back to Griffith whose fracture criterion, if we invoke Irwin's concept [42] of the stress intensity factor (SIF), K_I, can be represented in the modern form as

$$\frac{K_\mathrm{I}^2}{2E^*} = \mathcal{G}_\mathrm{c}, \tag{48}$$

where $\mathcal{G}_\mathrm{c}$ is the critical value of the energy release rate.

Schapery [43] extended Eq. (48) to the viscoelastic case as

$$\frac{1}{2E^*_\infty}\int_{t_0}^{t} \Phi(t-\tau)\frac{\mathrm{d}K_\mathrm{I}^2(\tau)}{\mathrm{d}\tau}\,\mathrm{d}\tau = \mathcal{G}_\mathrm{c}, \tag{49}$$

where t_0 is the time moment when the compressive stress (negative SIF) turns to tensile stress (positive SIF). It is to note here that the time-dependent fracture criteria similar to Eq. (49) have been used in a number of studies [20,44,45] related to adhesive fibrillar systems.

For the simplicity's sake (in order to understand the time-dependent detachment of an individual micropillar), let us now consider the case of adhesive frictionless contact of a flat-ended cylindrical indenter of radius b with an *elastic* half-space, when the force–displacement relation $P_j = 2E^* b\delta_j$ is linear. Here, δ_j and P_j are the indenter displacement and the contact force, respectively. Then, it can be shown (see, e.g., [46,47]) that the contact SIF is given by

$$-K_\mathrm{I}^j = \frac{E^*}{\sqrt{\pi b}}\delta_j = \frac{P_j}{2\sqrt{\pi}b^{3/2}}. \tag{50}$$

Since the contact radius b is a constant, Eq. (50) can be generalized for the viscoelastic case in a straight-forward manner as

$$-K_\mathrm{I}^j(t) = \frac{P_j(t)}{2\sqrt{\pi}b^{3/2}} \simeq \frac{A_\mathrm{e}}{2\sqrt{\pi}b^{3/2}}p(\mathbf{x}^j,t), \tag{51}$$

where the asymptotic relation (21) has been taken into account.

The substitution of the right-hand side of (51) into Eq. (49) yields

$$\frac{A_\mathrm{e}^2}{8\pi E^*_\infty b^3}\int_{t_0(\mathbf{x})}^{t} \Phi(t-\tau)\frac{\partial}{\partial\tau}[p(\mathbf{x},\tau)]^2\,\mathrm{d}\tau = \mathcal{G}_\mathrm{c}, \tag{52}$$

where $t = t_0(\mathbf{x})$ is the time moment when the contact pressure $p(\mathbf{x},\tau)$ at the point $\mathbf{x}$ turns from positive (compressive stress) to negative (tensile stress) values.

To this end, a rather specific contact configuration (indenter/substrate) was assumed for an individual fibril. However, to cover a general case, we recast Eq. (52) as follows:

$$\frac{\chi}{bE^*_\infty}\int_{t_0(\mathbf{x})}^{t} \Phi(t-\tau)\frac{\partial}{\partial\tau}[p(\mathbf{x},\tau)]^2\,\mathrm{d}\tau = \mathcal{G}_\mathrm{c}. \tag{53}$$

Here, χ is a dimensionless empirical parameter that depends on the area density of the fibril distribution as well as the material mismatch between the fibrils and the substrate.

5.2. Contact radius evolution

In what follows, we consider the case of displacement-controlled loading and unloading. To fix the ideas, we assume the regime of constant retraction velocity, V. Thus, the variation of the punch displacement can be represented as

$$\delta_0(t) = \delta_{00}\mathcal{H}(t) - V(t-t_\mathrm{m})_+, \tag{54}$$

so that the retraction velocity is given by $\dot{\delta}_0(t) = -V$ for $t > t_\mathrm{m}$.

The substitution of (54) into Eq. (42) yields

$$\frac{\bar{c}_0}{E^*_\infty}p(r,t) = \Psi(t)\Big(\delta_{00} - \frac{r^2}{2\mathrm{R}}\Big)_+ - V\int_{t_\mathrm{m}}^{t} \Psi(t-\tau)\,\mathrm{d}\tau, \tag{55}$$

where $r \le a(t)$ and $t > t_\mathrm{m}$.

We observe that while the first term on the right.hand side of Eq. (55) is positive, the second term is strictly negative for any $t > t_\mathrm{m}$. Moreover, the integral in (55) equals $\int_0^{t-t_\mathrm{m}} \Psi(\tau')\,\mathrm{d}\tau'$, and therefore, it is an increasing function of the time variable t.

Let $t_0(r)$ denote the time moment $t = t_0(r)$ when the contact pressure $p(r,t)$ at the points with the polar radius r vanishes. According to Eq. (52), for $r < a_\mathrm{m}$, the function $t_0(r)$ is determined as the root of the equation

$$\Psi(t_0)\Big(\delta_{00} - \frac{r^2}{2\mathrm{R}}\Big)_+ - V\int_0^{t_0-t_\mathrm{m}} \Psi(\tau')\,\mathrm{d}\tau' = 0. \tag{56}$$

By returning to the detachment criterion (53) and applying it to the case of circular contact, let us transform its integral as follows:

$$\int_{t_0}^{t} \Phi(t-\tau)\frac{\partial}{\partial\tau}[p(r,\tau)]^2\,\mathrm{d}\tau = \int_{t_0}^{t} \Phi'(t-\tau)[p(r,\tau)]^2\,\mathrm{d}\tau + \Phi(0)[p(r,t)]^2 - \Phi(t-t_0)[p(r,t_0)]^2. \tag{57}$$

Now, taking into account that $p(r,t_0)=0$ by the definition of $t_0(r)$, in view of (57), we can simplify the detachment criterion as

$$\Phi(0)[p(r,t)]^2 + \int_{t_m}^{t} \Phi'(t-\tau)\big(-p(r,\tau)\big)_+^2\,\mathrm{d}\tau = \frac{bE_\infty^*}{\chi}\mathcal{G}_c. \tag{58}$$

Let us emphasize that Eq. (58) does not explicitly contain the unknown variable t_0 that satisfies Eq. (56). The substitution of $a(t)$ for r in Eq. (58) leads to the following equation for the contact radius:

$$\Phi(0)[p(a(t),t)]^2 + \int_{t_m}^{t} \Phi'(t-\tau)\big(-p(a(t),\tau)\big)_+^2\,\mathrm{d}\tau = \frac{bE_\infty^*}{\chi}\mathcal{G}_c, \tag{59}$$

where the contact pressure $p(r,t)$ is given by formula (55), so that

$$\frac{\bar{c}_0}{E_\infty^*}p(a(t),\tau) = \Psi(\tau)\Big(\delta_{00} - \frac{a^2(t)}{2\mathsf{R}}\Big) - V\int_{t_m}^{\tau}\Psi(\tau-\tau')\,\mathrm{d}\tau'. \tag{60}$$

We note that $(2\mathsf{R}\delta_{00}-a^2(t))_+ = 2\mathsf{R}\delta_{00}-a^2(t)$ for $a(t)<a_m=\sqrt{2\mathsf{R}\delta_{00}}$.

5.3. Debonding incubation time

Since non-adhesive loading is assumed, the contact zone achieved to the time moment $t=t_m$ will remain fixed during some initial time interval, $t\in(t_m,t_{inc})$, which will be called the interval of incubation time. The reason for its existence is that some time is needed for the contact stress to grow up to some critical value $p(a_m,t_{inc})$ of the contact pressure at the contact contour $r=a_m$, starting from the zero value $p(a_m,t_m)=0$ (see Eq. (55)).

According to Eqs. (53) and (55), the incubation time for adhesive fracture $\Delta t_{inc}=t_{inc}-t_m$ is determined by the equation

$$\int_{t_m}^{t_{inc}} \Phi(t-\tau)\Psi(\tau-t_m)\int_{t_m}^{\tau}\Psi(\tau-\tau')\,\mathrm{d}\tau'\mathrm{d}\tau = \frac{b\bar{c}_0^2}{2\chi E_\infty^* V^2}\mathcal{G}_c. \tag{61}$$

We note that the right-hand side of Eq. (61) has the physical dimension of time squared.

Because both functions $\Phi(t)$ and $\Psi(t)$ are positive, the double integral on the left-hand side of Eq. (61) is a monotonically increasing function of t_{inc}. This means that the value of t_{inc} decreases as the retraction velocity V increases. In the opposite way (when approaching the limit of quasi-static detachment), the trend holds as well; however, it is *a priori* not evident that, generally speaking, the integral on the left-hand side of Eq. (61) can grow to infinity as time tends to infinity.

Let E_0^* denote the instantaneous reduced elastic modulus. We put $\rho=E_\infty^*/E_0^*$. Then by the well-known physical arguments (see, e.g., [48]), we have that the normalized creep function $\Phi(t)$ monotonically increases from ρ to 1 as $t\to\infty$, while the normalized relaxation function $\Psi(t)$ monotonically decreases from $1/\rho$ to 1. Therefore, the left-hand side of Eq. (61) can be easily estimated by $(\rho/2)(t_{inc}^2-t_m^2)$ from below and $(1/2\rho)(t_{inc}^2-t_m^2)$ from above. Hence, for any positive value of the right-hand side of Eq. (61), there is a unique solution $t_{inc}>t_m$, and the incubation time Δt_{inc} decreases to zero as the retraction velocity V tends to infinity.

Thus, the apparent contact radius $a(t)$ remains constant, i.e., $a(t)\equiv a_m$, during the incubation time interval (t_m,t_{inc}) and starts to decrease for $t>t_{inc}$.

5.4. Quasi-static adhesive rate-independent unloading

As evident from the previous analysis, a simple limit as V tends to zero is not possible. Indeed, Eq. (55) in the limit $V=0$ reduces to the relation $(\bar{c}_0/E_\infty^*)p(r,t)=\Psi(t)(\delta_{00}-r^2/(2\mathsf{R}))_+$, which should be further simplified to the quasi-static solution $p(r,t)=(E_\infty^*/\bar{c}_0)(\delta_{00}-r^2/(2\mathsf{R}))_+$, assuming that $\Psi(t)\simeq 1$ or, which is the same, $E^*(t)\simeq E_\infty^*$. However, the obtained solution should be termed 'static', as it corresponds to the moment of maximum indentation. The quasi-static approximation follows from Eq. (55) under the condition $\Psi(t)\simeq 1$ in the form

$$\frac{\bar{c}_0}{E_\infty^*}p(r,t) \simeq \Big(\delta_{00}-\frac{r^2}{2\mathsf{R}}\Big)_+ - V(t-t_m), \tag{62}$$

where the time variable t is treated as a time-like parameter, and, in view of (54), we have $V(t-t_m)=\delta_0-\delta_{00}$ for $t>t_m$.

Correspondingly, assuming that $\Phi(t)\simeq 1$ in the quasi-static loading, we reduce the adhesive fracture criterion (53) to the form

$$\frac{\chi}{bE_\infty^*}\int_{t_0(r)}^{t}\frac{\partial}{\partial\tau}[p(r,\tau)]^2\,\mathrm{d}\tau = \mathcal{G}_c,$$

from where, in view of the conditions $p(r,t_0)=0$ and $r=a(t)$, it follows that

$$\frac{\chi}{bE_\infty^*}[p(a,t)]^2 = \mathcal{G}_c. \tag{63}$$

The quasi-static adhesion fracture criterion (63) is equivalent to the simple condition that the average contact pressure $p(r,t)$ on the apparent contact contour $r=a(t)$ reaches some critical value, i.e., $p(a(t),t)=-p_c$ and $p_c=\sqrt{bE_\infty^*\mathcal{G}_c/\chi}$.

In light of the homogenization relation (51), the homogenized adhesion criterion $p(\mathbf{x},t)=-p_c$ applied at the point $\mathbf{x}=\mathbf{x}^j$ is equivalent to the adhesion criterion $P_j(t)=-P_c$ for the jth fibril, which also can be equivalently reformulated as $\delta_j(t)=-\delta_c$, where P_c and δ_c are the critical values for the contact force and the fibril's tip displacement, respectively.

We note that the adhesion fracture criterion $\delta_j(t)=-\delta_c$ is equivalent to the criterion of the critical fibril elongation that was adopted in [49].

5.5. Approximate solution for the contact radius during fast unloading after long dwell time

Assuming that t_m is very large compared to the primary relaxation time, τ_R, we can simplify Eq. (55) as

$$\frac{\bar{c}_0}{E_\infty^*}p(r,t) \simeq \Big(\delta_{00}-\frac{r^2}{2\mathsf{R}}\Big)_+ - V\int_{t_m}^{t}\Psi(t-\tau)\,\mathrm{d}\tau, \tag{64}$$

where $r\le a(t)$ and $t>t_m$.

Now, the assumption of fast unloading implies that we can make use of the approximations

$$\Psi(t)\simeq\frac{1}{\rho}(1-\eta t),\quad \Phi(t)\simeq\rho(1+\eta t), \tag{65}$$

where η is a constant having the dimension of inverse time, and $1/\eta$ is proportional to τ_R.

Correspondingly, we can introduce a small parameter

$$\epsilon=\frac{\eta\delta_{00}}{V}. \tag{66}$$

In accord with asymptotic relation (64), Eq. (56) now takes the form

$$\int_0^{t_0-t_m}\Psi(\tau')\,\mathrm{d}\tau' \simeq \frac{\delta_{00}}{V}\Big(1-\frac{r^2}{a_m^2}\Big), \tag{67}$$

from where, in view of (65), we find that

$$\frac{t_0-t_m}{\tau_R}\simeq\epsilon\rho\Big(1-\frac{r^2}{a_m^2}\Big). \tag{68}$$

The substitution of (65) into Eq. (61) yields in the leading asymptotic term

$$\frac{t_{\rm inc}-t_{\rm m}}{\tau_{\rm R}} \simeq \epsilon\sqrt{\frac{\rho b\mathcal{G}_{\rm c}}{\chi E_\infty}^*}\,\frac{\bar{c}_0}{\delta_{00}}. \tag{69}$$

Further, by differentiating Eq. (64) with respect to time, we obtain

$$\frac{\bar{c}_0}{E_\infty^*}\frac{\partial p(r,t)}{\partial t} \simeq -V\Psi(t-t_{\rm m}) \simeq -\frac{V}{\rho}[1-\eta(t-t_{\rm m})], \tag{70}$$

where additionally the first asymptotic formula (65) was utilized.

Now, returning to formula (64), we rewrite it in the form

$$\frac{\bar{c}_0}{E_\infty^*}p(r,t) \simeq \Big(\delta_{00}-\frac{r^2}{2\mathsf{R}}\Big)_+ - V\int_0^{t_0-t_{\rm m}}\Psi(\tau')\,{\rm d}\tau' - V\int_{t_0-t_{\rm m}}^{t-t_{\rm m}}\Psi(\tau')\,{\rm d}\tau',$$

which, in view of (67) and (65), can be further simplified as

$$\frac{\bar{c}_0}{E_\infty^*}p(r,t) \simeq -V\int_{t_0-t_{\rm m}}^{t-t_{\rm m}}\Psi(\tau')\,{\rm d}\tau' \simeq -\frac{V}{\rho}(t-t_0). \tag{71}$$

We observe that the right-hand side of the asymptotic relation (71) still depends on the radial coordinate r via the function $t_0(r)$. So, in view of (68), formula (71), applied for $r=a(t)$, can be recast in the final form

$$\frac{\bar{c}_0}{E_\infty^*}p(r,\tau) \simeq \delta_{00}\Big(1-\frac{a^2}{a_{\rm m}^2}\Big) - \frac{V}{\rho}(\tau-t_{\rm m}), \tag{72}$$

where $a(t)<a_{\rm m}$.

As we already know (see Section 5.3), $a(t)\equiv a_{\rm m}$ for $t\in(t_{\rm m},t_{\rm inc})$. Therefore, Eq. (71) should be applied for $t>t_{\rm inc}$, and, in view of (65), we simplify it as

$$[p(a,t)]^2 + \eta\int_{t_{\rm m}}^{t}(-p(a,\tau))_+^2\,{\rm d}\tau' \simeq \frac{bE_\infty^*}{\rho\chi}\mathcal{G}_{\rm c}. \tag{73}$$

Taking into account the approximate solution (72), we find that

$$\frac{\bar{c}_0^2}{(E_\infty^*)^2}\int_{t_{\rm m}}^{t}(-p(a,\tau))_+^2\,{\rm d}\tau' = \int_{\tau_{\rm m}}^{t-t_{\rm m}}\Big[\frac{V}{\rho}\tau' - \delta_{00}\Big(1-\frac{a^2}{a_{\rm m}^2}\Big)\Big]^2{\rm d}\tau', \tag{74}$$

where we have introduced the notation

$$\tau_{\rm m} = \frac{\rho\delta_{00}}{V}\Big(1-\frac{a^2}{a_{\rm m}^2}\Big). \tag{75}$$

In view of (75), Eq. (74) can be rewritten as

$$\frac{\bar{c}_0^2}{(E_\infty^*)^2}\int_{t_{\rm m}}^{t}(-p(a,\tau))_+^2\,{\rm d}\tau' = \frac{V^2}{\rho^2}\int_{\tau_{\rm m}}^{t-t_{\rm m}}(\tau'-\tau_{\rm m})^2\,{\rm d}\tau' = \frac{V^2}{3\rho^2}[t-t_{\rm m}-\tau_{\rm m}]^3. \tag{76}$$

Thus, collecting formulas (72) and (76), we transform Eq. (73) as

$$[\tau_{\rm m}-(t-t_{\rm m})]^2 + \frac{\eta}{3}[t-t_{\rm m}-\tau_{\rm m}]^3 = \frac{\bar{c}_0^2\rho b\mathcal{G}_{\rm c}}{\chi E_\infty^* V^2}, \tag{77}$$

where again the short-hand notation (75) has been utilized.

Since $\eta(t-t_{\rm m}-\tau_{\rm m})$ is of the order ϵ (cf. the asymptotic relations (70) and (68)), in the leading asymptotic term Eq. (77) implies that

$$t-t_{\rm m}-\frac{\rho\delta_{00}}{V}\Big(1-\frac{a^2}{a_{\rm m}^2}\Big) \simeq \frac{\bar{c}_0}{V}\sqrt{\frac{\rho b\mathcal{G}_{\rm c}}{\chi E_\infty}^*}, \tag{78}$$

from where, in view of (69), we find the evolution of the contact radius in the form

$$a(t) \simeq a_{\rm m}\sqrt{1-\frac{V}{\rho\delta_{00}}(t-t_{\rm inc})}. \tag{79}$$

Finally, we note that the variation of the contact force upon unloading can be evaluated from the equation

$$\frac{\bar{c}_0}{\pi E_\infty^*}Q(t) = a^2(t)\Big(\delta_{00}-\frac{a^2(t)}{4\mathsf{R}}\Big)\Psi(t) - a^2(t)V\int_{t_{\rm m}}^{t}\Psi(t-\tau)\,{\rm d}\tau, \tag{80}$$

which follows from Eq. (41).

5.6. A lower-bound estimate for the pull-off force under fast unloading

Since we are interested in what happens with $Q(t)$ for $t>t_{\rm m}$, we rearrange Eq. (80) as

$$\begin{aligned}\frac{\bar{c}_0}{\pi E_\infty^*}Q(t) = {}& \frac{\bar{c}_0}{\pi E_\infty^*}Q(t_{\rm m}) + a^2(t)\Big(\delta_{00}-\frac{a^2(t)}{4\mathsf{R}}\Big)\Psi(t)\\ & - a_{\rm m}^2\Big(\delta_{00}-\frac{a_{\rm m}^2}{4\mathsf{R}}\Big)\Psi(t_{\rm m})\\ & + a^2(t)\int_{t_{\rm m}}^{t}\Psi(t-\tau)\dot{\delta}_0(\tau)\,{\rm d}\tau.\end{aligned} \tag{81}$$

In the case of fast unloading after along dwelling time, we have $\Psi(t_{\rm m})\simeq 1$ and the difference $\Psi(t)-\Psi(t_{\rm m})$ is small for $t>t_{\rm m}$ and large $t_{\rm m}$, and therefore, formula (81) can be simplified as

$$\begin{aligned}\frac{\bar{c}_0}{\pi E_\infty^*}Q(t) \simeq {}& \frac{\bar{c}_0}{\pi E_\infty^*}Q(t_{\rm m}) + \delta_{00}(a^2(t)-a_{\rm m}^2) - \frac{1}{4\mathsf{R}}(a^4(t)-a_{\rm m}^4)\\ & + a^2(t)V\int_{t_{\rm m}}^{t}\Psi(t-\tau)\dot{\delta}_0(\tau)\,{\rm d}\tau.\end{aligned} \tag{82}$$

During the debonding incubation time, we have $a(t)\equiv a_{\rm m}$ and $\dot{\delta}_0(t)=-V$, so that

$$\frac{\bar{c}_0}{\pi E_\infty^*}Q(t) \simeq \frac{\bar{c}_0}{\pi E_\infty^*}Q(t_{\rm m}) - a_{\rm m}^2V\int_{t_{\rm m}}^{t}\Psi(t-\tau)\,{\rm d}\tau, \quad t\in(t_{\rm m},t_{\rm inc}). \tag{83}$$

In view of (82), (83), and the zeroth-order approximation $\Psi(t-\tau)\simeq 1/\rho$, the total contact force reached to the end of the incubation interval can be estimated as

$$Q(t_{\rm inc}) \simeq Q(t_{\rm m}) - \frac{\pi E_\infty^*}{\bar{c}_0}\frac{Va_{\rm m}^2}{\rho}(t_{\rm inc}-t_{\rm m}). \tag{84}$$

Thus, taking into account the asymptotic estimate (69) for the incubation time, we can rewrite formula (84) in the form

$$Q(t_{\rm inc}) \simeq Q(t_{\rm m}) - \pi E_\infty^* a_{\rm m}^2\sqrt{\frac{b\mathcal{G}_{\rm c}}{\rho\chi E_\infty}^*}. \tag{85}$$

For extended dwell times, in view of (35), we have

$$Q(t_{\rm m}) = \frac{\pi\mathsf{R}E_\infty^*}{\bar{c}_0}\delta_{00}^2 = \frac{\pi E_\infty^* a_{\rm m}^4}{4\mathsf{R}\bar{c}_0}. \tag{86}$$

In the case of strong adhesion (when the ratio $b\mathcal{G}_{\rm c}/E_\infty^*$ is large), the second term of the right-hand side of Eq. (85) will be dominant, and thus, formula (85) provides an estimate for the pull-off force from below.

We also note that

$$\delta_0(t_{\rm inc}) \simeq \delta_{00} - \bar{c}_0\sqrt{\frac{\rho b\mathcal{G}_{\rm c}}{\chi E_\infty^*}}. \tag{87}$$

After the incubation time, according to the asymptotic solution (79), the contact radius decreases such that

$$\dot{a}(t) \simeq -\frac{V}{2\rho\delta_{00}}\frac{a_{\rm m}^2}{a(t)}, \quad t\in(t_{\rm inc},t_{\rm end}), \tag{88}$$

where

$$t_{\rm end} \simeq t_{\rm inc} + \frac{\rho\delta_{00}}{V}. \tag{89}$$

In the case of strong adhesion, it can be shown that $Q(t)>Q(t_{\rm inc})$ within the interval $(t_{\rm inc},t_{\rm end})$, meaning that $Q(t_{\rm inc})$ coincides with pull-off force upon fast unloading.

6. Discussion and conclusions

In Section 2, we presented an exact analysis of a simple homogenization model for the adhesive contact of a viscoelastic Winkler-type foundation. This model was originally formulated in [22] and solved numerically. The experimental verification of this model and of more advanced analytical models constructed herein (or, more precisely,

the investigation of their applicability for fitting experimental data) clearly requires a separate study. Nonetheless, it is worth noting that the corresponding purely elastic model [49] (to which the viscoelastic model reduces in the quasistatic limit) can, as shown in [50], be employed within certain parameter ranges, provided that both bulk and surface viscoelastic effects are negligible.

By neglecting the effect of the backing layer (which can be crucial for bioinspired interfaces depending on its relative thickness) and by introducing the concept of debonding incubation time, the constructed homogenized model based on the Schapery model allows for an analytical approximation of the pull-off force. This approximation holds under conditions of strong adhesion and rapid unloading after a long contact time. However, due to its evident technical complexity, the general contact problem, which includes the backing layer effect and arbitrary loading protocols, requires a sophisticated numerical approach.

While several simplifying assumptions have been introduced to enhance clarity, many of them can be relaxed. For example, the punch shape function (see Eq. (24)) can be chosen in a more general axisymmetric form, such as a monomial (power-law) (see, e.g., [51]). However, it should be borne in mind that the applicability of the homogenized model requires the apparent contact area to be much larger than the periodic cell, and that it contains a sufficiently large number of fibrils. The homogenized model is also not suitable for sharp punches (such as conical or pyramidal), as it does not accurately capture the contact interactions near the punch apex. However, for a blunt conical punch — provided the applicability conditions outlined above are satisfied — the singularity effect can be safely neglected.

The convexity of the punch is not a significant concern; however, removing this constraint — even in the axisymmetric case — can result in non-connected contact zones. In other words, multiple apparent contact areas may appear, which can merge or separate during indentation or detachment.

The most critical assumption involves the cylindrical shape of the fibril tips, which is closely tied to the adopted model for individual fibril detachment based on Schapery's fracture criterion (49). The latter assumes that the individual contact zone — formed by a single cylindrical micropillar — remains circular until the moment of detachment, which occurs instantaneously when the contact SIF-based energy release rate reaches its critical value, $\mathcal{G}_c$. This adhesion characteristic is assumed to be constant, implying that the adhesion is rate-independent.

It is worth noting that adhesive detachment experiments [52–54] using cylindrical indenters retracted at constant velocity reveal that the contact area begins to shrink to an unstable, small region shortly after the critical moment predicted by the adhesion fracture criterion (49). Consequently, the proposed modeling framework omits this brief transient phase during fibril detachment. In general, this phenomenon is often neglected for small fibrils, as its effect is difficult to evaluate in a consistent and reproducible manner.

Moreover, changing the fibril shape — for example, to a hemispherical form — necessitates a modification of the adhesive fracture criterion (49), since the individual contact area will vary throughout the entire indentation/retraction cycle. In such cases, applying the Gent–Schultz model [55] for rate-dependent adhesion may be a suitable alternative.

A separate study is required to account for the bending deformation of micropillars, particularly when interaction with the backing layer is involved, as this can soften the contact between the micropillar and the substrate. A key issue is that the adhesive fracture criterion (49) assumes axisymmetry in the singular stress–strain field near the micropillar edge. However, this assumption is incompatible with micropillar bending, which can occur even with a rigid substrate — for instance, due to local inclination of the punch surface. It is generally believed that for normal (vertical) indentation by a relatively shallow punch — where the punch radius R is much larger than the characteristic size $\sqrt{A_c/\pi}$ of the periodic cell — the effect of micropillar bending is minimal. However, this assumption does not hold under tangential or torsional loading conditions.

Finally, the assumption of linear viscoelasticity, defined by Eqs. (1) and (11)–(13), can be a significant limitation when modeling many biological materials.

Regarding a possible experimental verification of the constructed homogenized model for a fibrillar surface of a thin viscoelastic substrate (that is, without strong backing layer interaction) it is fruitful to compare formulas (6) and (79) for the apparent contact radius variation. With this aim, we rewrite these formulas as follows:

$$\frac{a_m^2 - a^2(t)}{a_m^2} \simeq \frac{V}{\delta_{00}}(t - t_{inc})\gamma, \tag{90}$$

where $\gamma = 1/\rho$ for the Schapery model and $\gamma = 1$ for the Shrimali–Lopez-Pamies model.

It should be noted that, while formula (6) is exact in the developed mathematical modeling framework, we still keep the symbol of approximate equality in (90) to highlight the fact that this result has been obtained from the homogenized asymptotic model. The scaling relation (90) can be used for the analysis of the variation of the apparent contact radius.

As seen from the above analysis, the SLP and Schapery models for the adhesion of an individual viscoelastic fibril yield qualitatively similar results in both quasistatic and fast unloading cases. For slow detachment, both adhesion fracture criteria produce identical results (given proper model initialization), as the effect of viscoelasticity diminishes in the quasistatic limit. However, under fast unloading, the predictions of the two models differ quantitatively.

To conclude, our main result is the asymptotic model of rate-independent adhesion for a viscoelastic fibrillar surface developed using a homogenization approach. A comparison is made between the predictions of the Shrimali–Lopez-Pamies and Schapery-type adhesive detachment criteria for the variation of contact area upon fast unloading. A recommendation for the experimental verification of the adhesion fracture criterion for viscoelastic fibrillar interfaces has been proposed. Given the model simplifications outlined above, the derived analytical solutions must be applied with caution. While the theoretical framework developed here is based on well-established adhesion models and introduces no unphysical assumptions, it is not intended to be universal.

CRediT authorship contribution statement

I. Argatov: Writing – original draft, Methodology, Formal analysis. **A. Papangelo:** Writing – review & editing, Writing – original draft, Methodology, Funding acquisition, Formal analysis, Conceptualization.

Declaration of competing interest

The authors declare that they have no known competing financial interests or personal relationships that could have appeared to influence the work reported in this paper.

Acknowledgments

The authors were partly supported by the Italian Ministry of University and Research under the Programme "Department of Excellence" Legge 232/2016 (Grant No. CUP – D93C23000100001). A.P. was supported by the European Union (ERC-2021-STG, "Towards Future Interfaces With Tuneable Adhesion By Dynamic Excitation" – SURFACE, Project ID: 101039198, CUP: D95F22000430006). Views and opinions expressed are however those of the authors only and do not necessarily reflect those of the European Union or the European Research Council. Neither the European Union nor the granting authority can be held responsible for them.

Data availability

No data was used for the research described in the article.

References

[1] K. Autumn, A.M. Peattie, Mechanisms of adhesion in geckos, Integr. Comp. Biology 42 (6) (2002) 1081–1090.
[2] K. Autumn, Y.A. Liang, S.T. Hsieh, W. Zesch, W.P. Chan, T.W. Kenny, R. Fearing, R.J. Full, Adhesive force of a single gecko foot-hair, Nature 405 (6787) (2000) 681–685.
[3] M.D. Bartlett, A.B. Croll, D.R. King, B.M. Paret, D.J. Irschick, A.J. Crosby, Looking beyond fibrillar features to scale gecko-like adhesion, Adv. Mater. 24 (8) (2012) 1078–1083.
[4] L.F. Boesel, C. Greiner, E. Arzt, A. Del Campo, Gecko-inspired surfaces: a path to strong and reversible dry adhesives, Adv. Mater. 22 (19) (2010) 2125–2137.
[5] W. Shi, X. Cheng, K. Cheng, Gecko-inspired adhesives with asymmetrically tilting-oriented micropillars, Langmuir 38 (29) (2022) 8890–8898.
[6] C. Linghu, Y. Liu, X. Yang, D. Li, Y.Y. Tan, M.H.B. Mohamed Hafiz, M.F.B. Rohani, Z. Du, J. Su, Y. Li, et al., Fibrillar adhesives with unprecedented adhesion strength, switchability and scalability, Natl. Sci. Rev. 11 (10) (2024) nwae106.
[7] J. Zhao, N. Xia, L. Zhang, A review of bioinspired dry adhesives: From achieving strong adhesion to realizing switchable adhesion, Bioinspiration Biomim. (2024).
[8] M. Tricarico, M. Ciavarella, A. Papangelo, Enhancement of adhesion strength through microvibrations: Modeling and experiments, J. Mech. Phys. Solids 196 (2025) 106020.
[9] H. Shahsavan, B. Zhao, Bioinspired functionally graded adhesive materials: synergetic interplay of top viscous–elastic layers with base micropillars, Macromolecules 47 (1) (2014) 353–364.
[10] S. Sikdar, M.H. Rahman, A. Siddaiah, P.L. Menezes, Gecko-inspired adhesive mechanisms and adhesives for robots–a review, Robotics 11 (6) (2022) 143.
[11] G. Giordano, R.B.N. Scharff, M. Carlotti, M. Gagliardi, C. Filippeschi, A. Mondini, A. Papangelo, B. Mazzolai, Mechanochromic suction cups for local stress detection in soft robotics, Adv. Intell. Syst. 6 (12) (2024) 2400254.
[12] A.L. Hook, N.H. Voelcker, H. Thissen, Patterned and switchable surfaces for biomolecular manipulation, Acta Biomater. 5 (7) (2009) 2350–2370.
[13] C. Linghu, S. Zhang, C. Wang, K. Yu, C. Li, Y. Zeng, H. Zhu, X. Jin, Z. You, J. Song, Universal SMP gripper with massive and selective capabilities for multiscaled, arbitrarily shaped objects, Sci. Adv. 6 (7) (2020) eaay5120.
[14] M. Samri, J. Thiemecke, R. Hensel, E. Arzt, Application of machine learning to object manipulation with bio-inspired microstructures, J. Mater. Res. Technol. 27 (2023) 1406–1416.
[15] I. Argatov, Q. Li, V.L. Popov, Cluster of the Kendall-type adhesive microcontacts as a simple model for load sharing in bioinspired fibrillar adhesives, Arch. Appl. Mech. 89 (2019) 1447–1472.
[16] Y. Cheng, Z. Peng, S. Chen, A theoretical model of enhanced adhesion of bioinspired micropillar arrayed surfaces, J. Mech. Phys. Solids 186 (2024) 105592.
[17] Q. Wang, A. Papangelo, M. Ciavarella, H. Gao, Q. Li, Rapid detachment of a rigid sphere adhered to a viscoelastic substrate: An upper bound model incorporating maugis parameter and preload effects, J. Mech. Phys. Solids 196 (2025) 106028.
[18] A. Maghami, Q. Wang, M. Tricarico, M. Ciavarella, Q. Li, A. Papangelo, Bulk and fracture process zone contribution to the rate-dependent adhesion amplification in viscoelastic broad-band materials, J. Mech. Phys. Solids 193 (2024) 105844.
[19] W. Yang, X. Wang, P. Chen, X. Qiao, Viscoelastic adhesive contact between a sphere and a two-dimensional nano-wavy surface, Appl. Surf. Sci. 586 (2022) 152828.
[20] R. Li, D. Li, W. Zhang, Rate effects in detachment of a spherical probe from fibrillar adhesive surfaces, J. Mech. Phys. Solids 171 (2023) 105130.
[21] G. Violano, S. Dibitonto, L. Afferrante, Role of viscoelasticity in the adhesion of mushroom-shaped pillars, Bioinspiration & Biomimetics 19 (6) (2024) 066006.
[22] X.M. Liang, G.F. Wang, M. Ciavarella, Simple models of viscoelastic fibrillar adhesion to a rigid sphere, Extrem. Mech. Lett. 77 (2025) 102316.
[23] R.D. O'Rorke, T.W. Steele, H. Taylor, Bioinspired fibrillar adhesives: a review of analytical models and experimental evidence for adhesion enhancement by surface patterns, J. Adhes. Sci. Technol. 30 (4) (2016) 362–391.
[24] I.I. Argatov, T.A. Mel'nyk, Homogenization of a contact problem for a system of densely situated punches, Eur. J. Mech. A Solids 20 (1) (2001) 91–98.
[25] I. Argatov, Mechanics of heterogeneous adhesive contacts, Internat. J. Engrg. Sci. 190 (2023) 103883.
[26] V.I. Avilkin, V.M. Aleksandrov, E.V. Kovalenko, On using the more-accurate equations of thin coatings in the theory of axisymmetric contact problems for composite foundations, J. Appl. Math. Mech. 49 (6) (1985) 770–777.
[27] F.M. Borodich, B.A. Galanov, N.V. Perepelkin, D.A. Prikazchikov, Adhesive contact problems for a thin elastic layer: Asymptotic analysis and the JKR theory, Math. Mech. Solids 24 (5) (2019) 1405–1424.
[28] B. Shrimali, O. Lopez-Pamies, The "pure-shear" fracture test for viscoelastic elastomers and its revelation on griffith fracture, Extrem. Mech. Lett. 58 (2023) 101944.
[29] A. Ghatak, K. Vorvolakos, H. She, D.L. Malotky, M.K. Chaudhury, Interfacial rate processes in adhesion and friction, J. Phys. Chem. B 104 (17) (2000) 4018–4030.
[30] G. Carbone, B. Persson, Hot cracks in rubber: origin of the giant toughness of rubberlike materials, Phys. Rev. Lett. 95 (11) (2005) 114301.
[31] C.-Y. Hui, X. Xiao, M. Ciccotti, A rate dependent interface model for stick-slip fracture in adhesives and polymer glasses, Soft Matter 21 (2025) 5323–5336.
[32] M.R. Gecit, Axisymmetric contact problem for a semiinfinite cylinder and a half space, Internat. J. Engrg. Sci. 24 (8) (1986) 1245–1256.
[33] I. Argatov, Nonlinear elastic metafoundation as a model for adhesive micropatterned elastic interfaces, Internat. J. Engrg. Sci. 208 (2025) 104211.
[34] G.M. Guidoni, D. Schillo, U. Hangen, G. Castellanos, E. Arzt, R.M. McMeeking, R. Bennewitz, Discrete contact mechanics of a fibrillar surface with backing layer interactions, J. Mech. Phys. Solids 58 (10) (2010) 1571–1581.
[35] W.L. Noderer, L. Shen, S. Vajpayee, N.J. Glassmaker, A. Jagota, C.-Y. Hui, Enhanced adhesion and compliance of film-terminated fibrillar surfaces, Proc. R. Soc. A: Math. Phys. Eng. Sci. 463 (2086) (2007) 2631–2654.
[36] I.I. Argatov, I.A. Lyashenko, V.L. Popov, Adhesive sliding with a nominal point contact: Postpredictive analysis, Internat. J. Engrg. Sci. 200 (2024) 104055.
[37] I. Argatov, G. Mishuris, Contact Mechanics of Articular Cartilage Layers. Asymptotic Models, Springer, Cham, 2015.
[38] E.H. Lee, J.R.M. Radok, The contact problem for viscoelastic bodies, J. Appl. Mech. 27 (1960) 438–444.
[39] T.C.T. Ting, Contact problems in the linear theory of viscoelasticity, J. Appl. Mech. 35 (1968) 248–254.
[40] A. Papangelo, M. Ciavarella, Viscoelastic normal indentation of nominally flat randomly rough contacts, Int. J. Mech. Sci. 211 (2021) 106783.
[41] I.I. Argatov, I.A. Lyashenko, V.L. Popov, A cascade of adhesive sliding instabilities unveiled via a postpredictive analysis, J. Phys. D: Appl. Phys. 58 (18) (2025) 185304.
[42] G.R. Irwin, Analysis of stresses and strains near the end of a crack traversing a plate, J. Appl. Mech. 24 (1957) 361–364.
[43] R.A. Schapery, A theory of crack initiation and growth in viscoelastic media II. approximate methods of analysis, Int. J. Fract. 11 (1975) 369–388.
[44] H. Cheng, M. Li, J. Wu, A. Carlson, S. Kim, Y. Huang, Z. Kang, K.-C. Hwang, J. Rogers, A viscoelastic model for the rate effect in transfer printing, J. Appl. Mech. 80 (4) (2013) 041019.
[45] C. Liang, F. Wang, Z. Huo, B. Shi, Y. Tian, X. Zhao, D. Zhang, Pull-off force modeling and experimental study of PDMS stamp considering preload in micro transfer printing, Int. J. Solids Struct. 193 (2020) 134–140.
[46] H. Itou, V.A. Kovtunenko, K.R. Rajagopal, The Boussinesq flat-punch indentation problem within the context of linearized viscoelasticity, Internat. J. Engrg. Sci. 151 (2020) 103272.
[47] I.I. Argatov, Controlling the adhesive pull-off force via the change of contact geometry, Phil. Trans. R. Soc. A 379 (2203) (2021) 20200392.
[48] A.C. Pipkin, Lectures on Viscoelasticity Theory, Springer Science & Business Media, New York, 2012.
[49] M. Schargott, V.L. Popov, S. Gorb, Spring model of biological attachment pads, J. Theoret. Biol. 243 (1) (2006) 48–53.
[50] C. Greiner, A. Del Campo, E. Arzt, Adhesion of bioinspired micropatterned surfaces: effects of pillar radius, aspect ratio, and preload, Langmuir 23 (7) (2007) 3495–3502.
[51] F.M. Borodich, B.A. Galanov, L.M. Keer, M.M. Suarez-Alvarez, The JKR-type adhesive contact problems for transversely isotropic elastic solids, Mech. Mater. 75 (2014) 34–44.
[52] I.A. Lyashenko, V.L. Popov, Hysteresis in an adhesive contact upon a change in the indenter direction of motion: An experiment and phenomenological model, Tech. Phys. 66 (4) (2021) 611–629.
[53] I.I. Argatov, I.A. Lyashenko, V.L. Popov, Rate-dependent JKR-type decohesion of a cylindrical punch from an elastic substrate, Phys. Scr. 98 (5) (2023) 055905.
[54] A. Papangelo, M. Ciavarella, Detachment of a rigid flat punch from a viscoelastic material, Tribol. Lett. 71 (2) (2023) 48.
[55] A.N. Gent, J. Schultz, Effect of wetting liquids on the strength of adhesion of viscoelastic material, J. Adhes. 3 (4) (1972) 281–294.